Eleventh International Conference on CFD in the Minerals and Process Industries
CSIRO, Melbourne, Australia
7-9 December 2015

GAS - LIQUID FLOW IN WET ELECTROSTATIC PRECIPITATORS

Baoyu GUO[1,2*] Yinbiao SU[3], Ding YANG[3] and Aibing YU[2]

[1] School of Materials Science and Engineering, University of New South Wales, 2052, AUSTRALIA
[2] Department of Chemical Engineering, Monash University, Victoria 3800, AUSTRALIA
Experimental Technology Centre, Fujian Longking Co Ltd, Longyan, 364000, CHINA
*Corresponding author, E-mail address: baoyu@unsw.edu.au; bob.guo@monash.edu

ABSTRACT

The physics in a Wet type ESP is very complex. Based on Computational Fluid Dynamics (CFD), the present paper aims to simulate several important phenomena from the liquid spray generation to gas-droplet flow in electric field. A single passage between the adjacent plates is considered for the simulation domain. Firstly, the electric field intensity and ion charge density are solved locally around a corona emitter of a barbed wire electrode, which are applied to the entire ESP using periodic conditions. Next, the Euler-Lagrange method is used to simulate the gas-droplet flow. Water droplets are tracked statistically along their trajectories, together with evaporation and particle charging. Finally, the deposition density on the plate is taken as the input for the liquid film model. The liquid film is simulated separately using the homogenous Eulerian approach in ANSYS-CFX. In the current case, since the free surface of the thin water film is difficult to resolve, a special method is devised to determine the film thickness.

As parametric study, the variables considered include the nozzle pressure, initial spray spreading patterns (solid versus hollow spray) and plate wettability. The droplet emission rate and film thickness distribution are the results of interest. Main findings: Electric field has strong effect on the droplet trajectories. Hollow spray is preferred to solid spray for its lower droplet emission. The liquid film uniformity is sensitive to the plate wettability.

NOMENCLATURE

b electric mobility of ion charge
C_P specific capacity
D diffusivity coefficient
d particle diameter
$\mathbf{E}$,E electric field
$\mathbf{F}$ force
H_{ev} heat of evaporation
k turbulence kinetic energy
k_B Boltzmann constant
m mass
Nu Nusselt number
n_e number of charge on a particle
n_p particle number density
p pressure
q charge
q_e unit charge
S_ϕ source of generic variable
Sh Sherwood number
T temperature
t time
$\mathbf{u}$ velocity vectors
V electrical potential
W molecular weight
X mole fraction
κ dielectric constant
ε_0 electrical permittivity of vacuum
ρ density
ρ_{ion} space charge density
λ thermal conductivity
μ dynamic viscosity
μ_t turbulent eddy viscosity
ϕ generic variable (temperature, mass fraction)
Γ_ϕ diffusivity of generic variable
σ_ϕ turbulent Prandtl number of generic variable

Subscript
g gas phase
l liquid phase
p particle phase
dis dispersion

INTRODUCTION

Electrostatic Precipitator (ESP) can effectively remove fine particulate matters from many industry emission sources, such as exhaust gases from coal fired power plants (Schwinning, 1998). When using the traditional dry ESP, the main challenges come from the difficulty of collecting ultra-fine particles of high electric resistivity. As an alternative, the wet ESP technology applies water spray, or running water on the collecting plate (Yamamoto et al., 1998; Hitachi, 2015), so that the dust collected can be washed into the hopper without the use of mechanical rapping. The liquid film should be controlled such that minimum liquid is consumed without causing dust accumulation. Moreover, re-entrainment can be eliminated so that the Wet ESP allows a much higher gas velocity, which would make the design more compact compared with the traditional dry ESP. Introduction of liquid spray also changes the gas flow condition (temperature and humidity) which affects favourably the electric field and particle charging, although the mechanism is yet to be understood.

Spray can generate mists and increase the moisture in the gas, which favors ultra-fine dust particle charging. For example, experimental results (Chen et al., 2014) showed that without fine water mist, nanoparticle collection efficiency was 67.9–92.9%, which was greatly enhanced to 99.2–99.7%, via a mechanism “condensational growth”, when the Wet ESP was operated with fine water mist.

Complicated transport phenomena are involved in such an ESP process, e.g., multi-scale, multiphase flows (gas, liquid and solid particle), multi-field (electric field, flow field and force field in dust cake formation) (Guo et al., 2013). The particle collection efficiency depends strongly on the gas flow, the behaviours of spray droplets, and the distribution of the liquid film. In this context, mathematical/ numerical simulations in terms of flows, heat and mass transports can provide the detailed process information related to the wet type ESP. The present paper reports the recent progress on the development of a comprehensive ESP model, with a particular objective to investigate the liquid phase flow.

MODEL DESCRIPTION

The model includes several steps or submodels that address the following specific phenomena respectively: (1) Electric field, (2) Atomization nozzle, (3) Gas-droplet flow and (4) Liquid film formation. Firstly, the electric field intensity and ion charge density are solved locally around a typical corona emitter, which are applied to the entire ESP using periodic conditions. Secondly, the LISA (Linearized Instability Sheet Atomisation) breakup equations for a flat liquid sheet (Senecal et al., 1999) is extended to the case of conical spray, in order to calculate the initial particle conditions right after atomization: particle size, locations and velocities. Next, the mixed Euler-Lagrange method is used as the model framework for gas-droplet flow. Both the electric field and gas flow are solved using a finite volume based solver ANSYS-CFX14. The liquid droplets are tracked statistically along their trajectories, together with particle charging. Finally, a so-called homogeneous two phase flow model along with free surface sharpening is used to simulate the liquid film on the plate. The wall mass flow density obtained from the particle tracking model is applied on the wall as the mass source. For lower computational cost, the simulation can be restricted to a near-wall layer, which should be thicker than the liquid film by an order of magnitude. The solution of the electric field and gas-dust particles flow has been detailed in previous works (Guo et al., 2014). However, the liquid/spray flow involves more complicated phenomena, e.g., droplet breakup, heat/mass transfer, evaporation and free surface, which pose new challenges to the modelling exercise. The major governing equations are given below.

Electric field is controlled by Poisson equation of electric potential and corona current continuity:

$$\nabla^2 V = -\rho_{ion}/\varepsilon_0 \tag{1}$$

$$\nabla \bullet (\rho_{ion} b\mathbf{E}) - D\nabla\rho_{ion}) = 0 \tag{2}$$

$$\mathbf{E} = -\nabla \mathrm{V} \tag{3}$$

Gas flow equations in steady state (including continuity, momentum and generic scalar equations) :

$$\nabla \cdot (\rho_g \mathbf{u}_g) = \dot{m} \tag{4}$$

$$\begin{aligned} &\nabla \cdot (\rho_g \mathbf{u}_g \otimes \mathbf{u}_g) = \nabla(p + \tfrac{2}{3}\rho_g k) + \\ &\nabla \cdot [(\mu + \mu_t)(\nabla \mathbf{u}_g + (\nabla \mathbf{u}_g)^{\mathrm{T}})] + \rho_{ion}\mathbf{E} \\ &- n_p \tfrac{1}{8} C_D \pi d_p^2 \rho_g \,|\, \mathbf{u}_g - \mathbf{u}_p \,|\, (\mathbf{u}_g - \mathbf{u}_p) \end{aligned} \tag{5}$$

$$\nabla \cdot (\rho_g \mathbf{u}_g \phi) = \nabla \cdot (\Gamma_\phi + \tfrac{\mu_t}{\sigma_\phi})\nabla\phi + S_\phi \tag{6}$$

Particle flow (including momentum, mass and temperature)

$$\begin{aligned} m_p \frac{d\mathbf{u}_p}{dt} &= \tfrac{1}{8} C_D \pi d_p^2 \rho_g \,|\, \mathbf{u}_g - \mathbf{u}_p \,|\, (\mathbf{u}_g - \mathbf{u}_p) \\ &+ \tfrac{1}{6}\pi d_p^3 \mathbf{g}(\rho_p - \rho_g) + n_e q_e \mathbf{E} + \mathbf{F}_{dis} \end{aligned} \tag{7}$$

$$m_p C_P \frac{dT_p}{dt} = \pi d_p \lambda Nu (T_g - T_p) + H_{ev} \frac{dm_p}{dt} \tag{8}$$

$$\frac{dm_P}{dt} = \pi d_p \rho D Sh \frac{W_l}{W_g} \ln\left(\frac{1 - X_S^V}{1 - X_{vap}^V}\right) \tag{9}$$

Ishii-Zuber Drag Model (Ishii and Zuber 1979) is chosen for the droplet-gas interaction force. Particle charging rate is calculated according to Lawless (1996) as,

$$\frac{dv}{d\tau_q} = \begin{cases} f(w)\dfrac{v - 3w}{\exp(v - 3w) - 1}, & v > 3w \\ \dfrac{3w}{4}\left(1 - \dfrac{v}{3w}\right)^2 + f(w), & -3w \le v \le 3w \\ -v + f(w)\dfrac{-v - 3w}{\exp(-v - 3w) - 1}, & v < -3w \end{cases} \tag{10}$$

where v,w and τ_q are dimensionless numbers as follow:

$$v = \frac{n_e q_e^2}{2\pi\varepsilon_0 d_p k_B T},\ w = \frac{\kappa_p}{\kappa_p + 2}\frac{E d_p q_e}{2 k_B T},\ \tau_q = \frac{b\rho_{ion} t}{\varepsilon_0},$$

$$f(w) = \min(1, (w + 0.475)^{-0.575}) \tag{11}$$

The above time rate equation for the overall charge is usually applied to a spherical solid particle, but its accuracy for droplet charging may need further investigation in the future. For this reason, it can be regarded as first order approximation when applied to a liquid droplet.

For the falling film modelling, the homogeneous two phase flow model, along with free surface sharpening, is used to simulate the liquid film on the plate. The governing momentum equation has the form,

$$\begin{aligned} &\nabla \cdot (\rho \mathbf{u}_l \otimes \mathbf{u}_l) = \nabla p + \\ &\nabla \cdot [\mu(\nabla \mathbf{u}_l + (\nabla \mathbf{u}_l)^{\mathrm{T}})] + \mathbf{F}_l \end{aligned} \tag{12}$$

where ρ and μ are the mean density and viscosity, respectively, averaged over the phases, $\boldsymbol{F}$ is the body force, including gravity and surface tension force.

The surface tension model used in ANSYS CFX is based on the Continuum Surface Force model of Brackbill et al. (1992). This model treats the surface tension force as a volume force concentrated over the finite volumes located at the interface. A Primary Fluid (the liquid phase) is denoted as α and a Secondary Fluid (the gas phase) is denoted as β. The surface tension force given by the Continuum Surface Force model is:

$$\mathbf{F}_{\alpha\beta} = \mathbf{f}_{\alpha\beta}\delta_{\alpha\beta} = -\sigma_{\alpha\beta}\kappa_{\alpha\beta}\mathbf{n}_{\alpha\beta}\delta_{\alpha\beta} \tag{13}$$

$$\kappa_{\alpha\beta} = \nabla \cdot \mathbf{n}_{\alpha\beta} \tag{14}$$

where σ is the surface tension coefficient, $\boldsymbol{n}_{\alpha\beta}$ is the interface normal vector pointing from the primary fluid to the secondary fluid (calculated from the gradient of a smoothed volume fraction). The $\delta_{\alpha\beta}$ term is called the

interface delta function, so that the surface tension force is active only near to the interface.

When the interface between the two fluids intersects a wall, it is possible to account for wall adhesion by specifying the contact angle, θ , which the interface makes with the wall through the primary fluid. The interface normal vector used for the calculations of both curvature and the surface tension force must satisfy the wall contact angle.

To save computational time, the simulation domain can be restricted to a narrow layer (say, 5mm) above the plate, but this should be far thicker than the water film to be solved. The wall mass flow density obtained from the particle tracking model is applied on the wall as the mass source.

RESULTS

The simulation domain is rectangular box of 2m high×1.656m wide×0.3m deep, representing a single pass-way between adjacent plates. The electrode wires are positioned horizontally and perpendicularly to the bulk flow. Three spray nozzles are placed 0.412 m above the electrode with spacing of 0.525m. Water of 25°C is injected from all the nozzles.

Spray nozzle

Nozzle B1/4AX-3 (WHIRLJET™) is designed to generate a hollow cone spray. Its outlet diameter is 2.4mm. According to the catalogue, as the injection pressure increases, the volumetric flow rate as well as the cone angle of the spray increases, while the droplet diameter, d_0, decreases. The theoretical nozzle model is intended to calculate the initial droplet conditions under given injection pressure and flowrate. The calculated results by the current model are compared with experimental data from the nozzle provider (Figure 1). It is found that the current model predictions are consistent with the experiment data for the mean particle size if the injection pressure is above 3 bar.

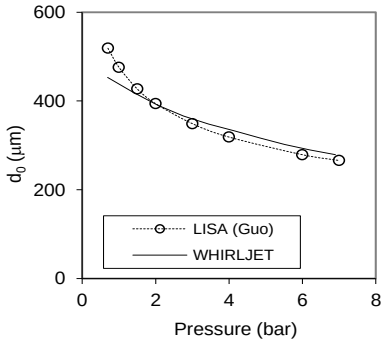

Figure 1. Droplet diameter VS injection pressure of nozzle.

Electric field

Figure 2 is the discharge electrode used - barbed wire (or needled wire) electrode. Each discharge electrode is made of barbed wire with an array of 10mm long needles, alternately arranged on two directions. Compared with a simple smooth wire electrode, the barbed wire offers the advantage of earlier onset voltage and stable corona generation. In the case with electric field, the voltage applied is assumed as 50kV, according to practical experiences for this wire-plate configuration. Figure 3 shows a typical electric field lines in side-view and the pattern of corona charge density in front-view facing the plate. The corona charge density has a discrete but regular pattern, corresponding to the alternate arrangement of the needles.

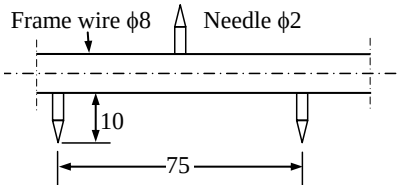

Figure 2. CS10A corona electrode considered.

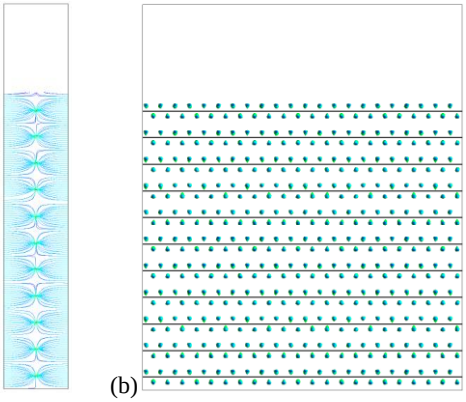

Figure 3. Electric field lines (a) and an iso-surface of corona charge density (b).

Typical gas-droplet flow

In the base case, the gas velocity is 3 m/s from the top boundary. Gas inlet temperature is 90°C and water initial temperature is 25°C. The initial moisture content of gas is 2% in mass fraction, corresponding to the saturation condition of the air at 25°C. This means that the moisture in the gas is under-saturated at elevated temperature, i.e., 4.55% in relative humidity at 90°C. The nozzle pressure is P_{inj}= 6 bar (gauge).

Figure 4 shows the trajectories of the droplets in the front-view facing the plates. The droplets, after being charged, turn their way toward the plate as they move down through the electric field. The particle temperature increases (by maximum 11 [K]), while their diameters decrease due to evaporation.

Figure 5 shows the velocity vectors, moisture content and temperature of gas. In the electric field downstream of the sprays, the velocity vectors show secondary flows that are caused by the electrostatic forces. Gas velocities in the spray concentrated region are higher due to the drag of the high speed droplets. Particularly, the temperature in the downstream region of the nozzle is lower than the surrounding. As an explanation, the nozzle body and liquid sheet would block the upstream fresh hot gas. It should be pointed out that the space occupied by the nozzle body is neglected. Moreover, a conical liquid sheet from the nozzle outlet to the breakup point is also ignored. Since this length scale is normally small compared with computational grid size, the gas flow at this region is most likely under-resolved. To solve this problem, in the cone-shaped volume enclosed by the water sheet, a large

resistance force is imposed to stop the gas flow locally. This special treatment is found to affect the downstream gas flow, heat mass/heat transfer in the near field, and leads to more sensible result.

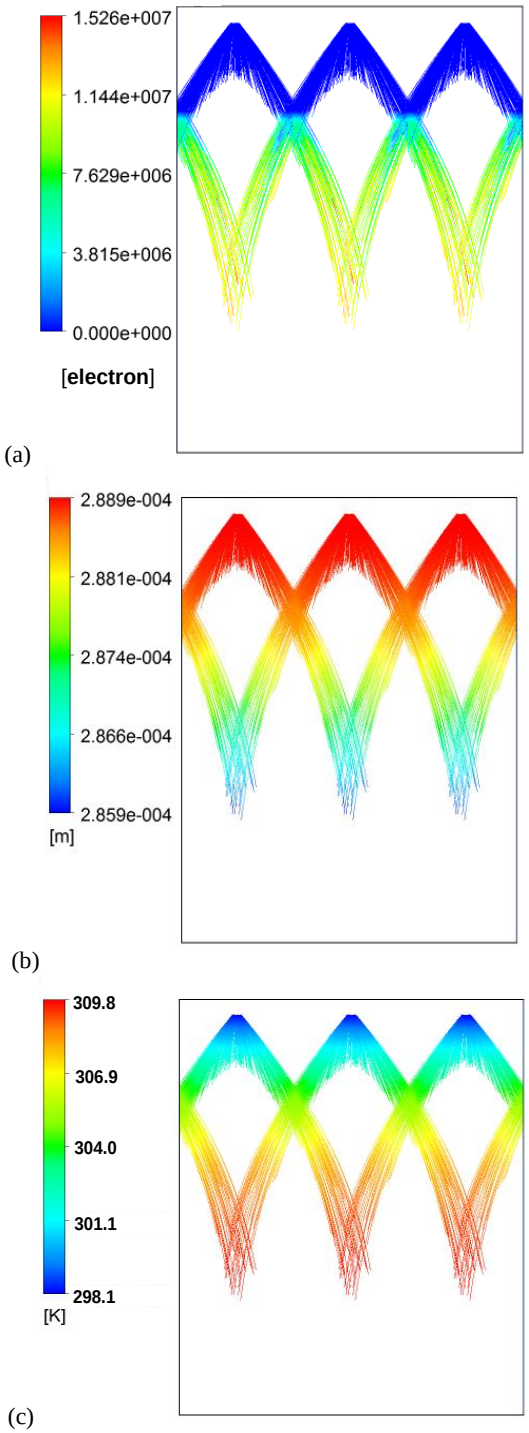

Figure 4. Trajectories of droplets with colour scaled to particle charge (a), diameter (b), and temperature (c) , respectively.

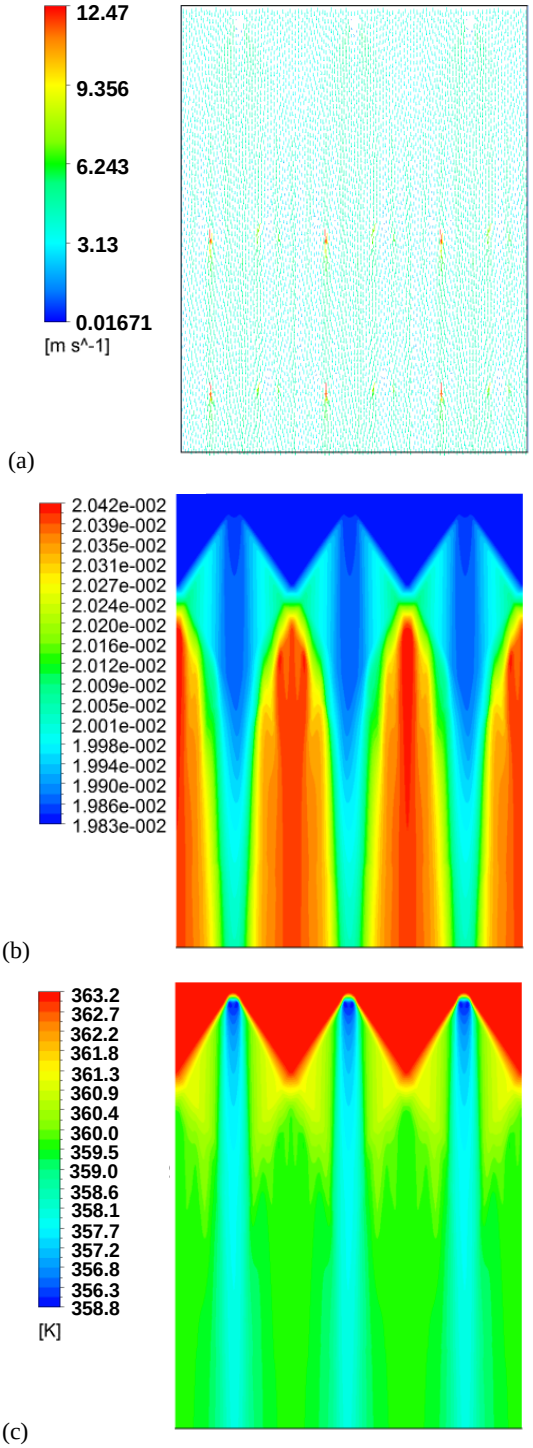

Figure 5. Distribution of gas velocity (a), moisture mass fraction (b), and temperature (c) in the plane passing the nozzles and electrodes.

The droplets have a strong momentum initially and tend to fall on a narrow band on the plate due to the hollow spray condition (Figure 6). The deposited droplets provide surface mass source as an input to the falling film model.

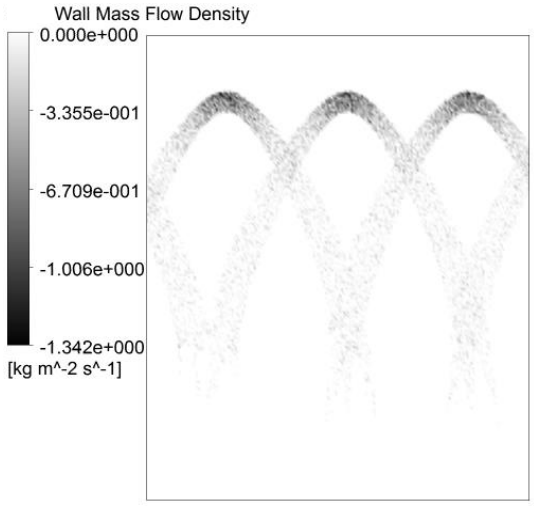

Figure 6. Deposition pattern of droplets on the plate**.**

Effect of electric field

In the case without electric field, droplets are subjected to gravity and drag force only. A droplet will deposit only if its initial momentum toward the plate is high enough to overcome the drag force during its residence time. Figure 7 shows significant proportion of droplets escaping through the bottom outlet (up to 16%). In the case with electric field switched on, almost all droplets are better charged and driven to the plate with few of them escaping from the domain considered. Note that the corona needles are currently parallel to the plate, which can be compared with another case where the needles are pointing to the plate perpendicularly (Guo et al., 2015). It is found that the current case is an improvement in terms of a lower droplet escaping rate.

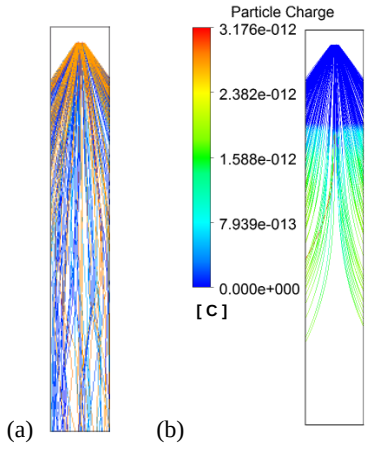

Figure 7. Side view of droplet trajectories for cases without electric field (a) and with electric field (b)**.**

Hollow cone spray versus solid cone spray

The solid cone spray is generated by increasing the dispersion angle from 10° to the full spray angle. For the case of solid cone spray, more droplets are injected in streamwise directions, thus have a smaller velocity component towards the plate. These particles tend to travel longer distance before settling on the plate; 3.3% droplets exit bottom outlet without collection. Those collected droplets collide with the plate in widespread points rather than focusing on a narrow band, as in the case of hollow cone spray. It can be seen that the initial momentum and direction of the spray droplets play an important role. It should be noted that the current study assumes mono-dispersed droplets from the nozzle, while poly-disperse droplets are very likely in reality. The behaviors of small droplets will be likely to deviate from the base case result. As the droplet size decreases, the initial momentum becomes smaller and the drag force acting on the droplet will play a more important role. As a consequence, small droplets will fall in the central part of the hollow cone.

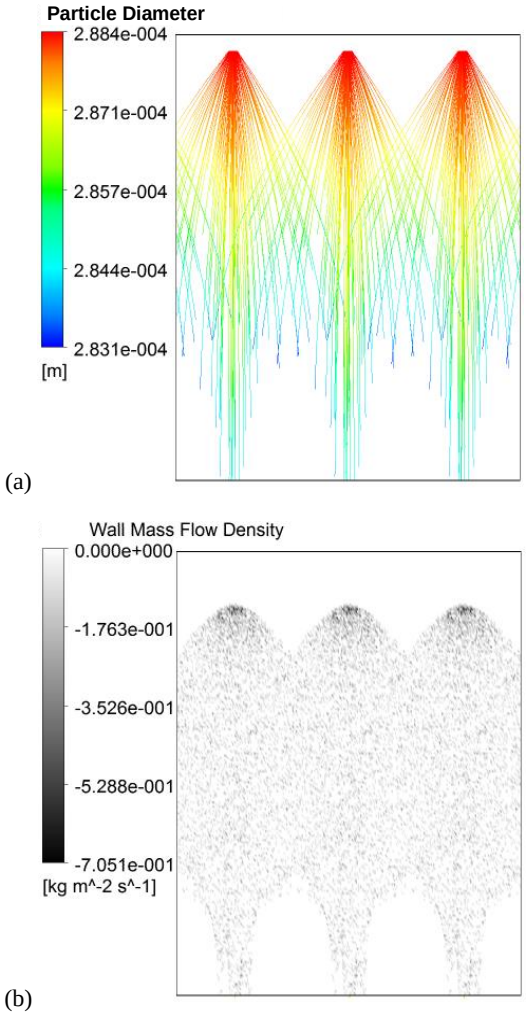

Figure 8. Trajectories of spray droplets (a) and deposition pattern (b) for the case of solid cone spray**.**

Liquid film

A uniform liquid (water) film is the ultimate goal for best removal efficiency of dust particles. The falling film formation is modelled by a two-fluid model. However, due to the computational cost, it is difficult to obtain a sharp free surface numerically. A post-processing method is needed to determine the film thickness. This is done by integrating volume fraction in the normal direction of the plate. Note, normally a free surface is determined by a cutting boundary at a critical volume fraction (e.g., 0.5). This simple method, in the current case of thin liquid film, gives rise to a large error, whereas the integration method guarantees the phase mass conservation, and is able to avoid the numerical uncertainty. The differences of the results can be seen clearly in Figure 9.

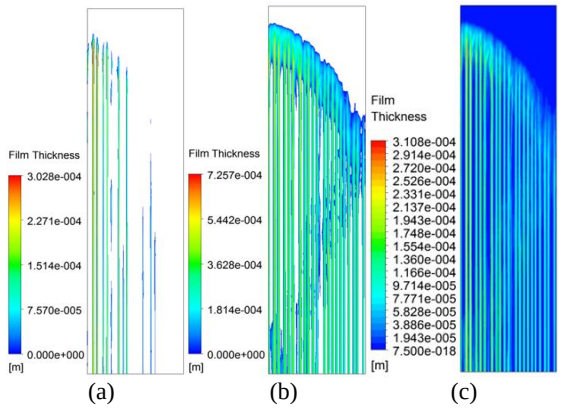

Figure 9. Determined liquid surface by (a), $V_f = 0.5$, (b), $V_f = 0.1$, and (c), integration of volume fraction**.**

The simulation result of the liquid film depends on gas velocity, droplet deposition rate and its distribution on the plate. Interfacial forces caused by surface tension, curvature and wall contact angle also play an important role if the liquid film is too thin and rough in surface shape. For a comparison, two cases are considered: (a) fully wetting wall and (b) partly wetting wall with contact angle of 40° (typical for stainless steel 316L). The liquid film predicted varies in thickness from zero up to 0.16 mm for the case of fully wetting wall (Figure 10(a)). For the case of partly wetting wall, a stripe pattern appears and the film becomes even less uniform, leaving a larger area of dry wall surface (Figure 10(a)), which would adversely affect the ESP performance.

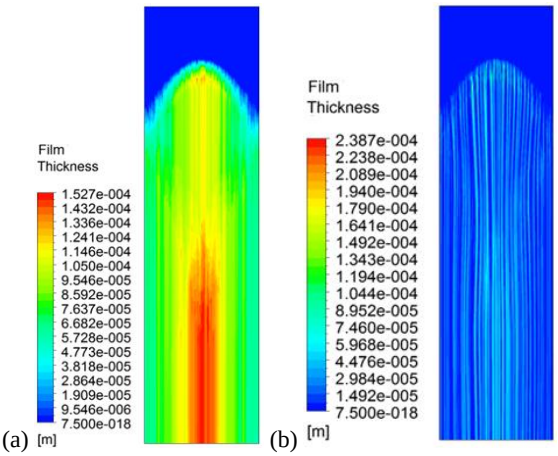

Figure 10. Contours of liquid film thickness showing the effect of contact angle on liquid film distribution. (a) θ=0°, (b)θ=20°.

CONCLUSION

A CFD based model with mixed numerical methods is developed to simulate the complicated liquid flow and other transport phenomena in electric field in wet ESP. The methods used include a theoretical nozzle model, Lagrangian particle tracking, and free surface simulation.

The main findings are: (a) The extended LISA model predicts the mean droplet size accurately. (b) Electric field has a strong effect on the droplet trajectories. With the corona needles parallel to the plate, the current electrode configuration is able to improve the droplet collection rate. (c) Hollow cone spray is better than a solid cone spray in droplets collection. (d) The plate wettability has significant effect on the liquid film uniformity.

The current model is able to generate detailed information on the coupled electric field, gas-liquid flow in the wet ESP, and will offer a tool for process optimization in terms of uniform liquid film and lower liquid consumption.

ACKNOWLEDGEMENTS

Financial support from Australian Research Council and Fujian Longking Co., Ltd are gratefully acknowledged. The first author likes to thank Prof David Fletcher (Leap) for his advice on particle charging in CFX.

REFERENCES

BRACKBILL, J.U, KOTHE, D.B. and ZEMACH, C., (1992), "A continuum method for modelling surface tension", *J. Computational Physics*, **100**, 335-354.

CHEN,T.M., TSAI, C.J., YAN, S.Y. and LI, S.N., (2014), "An efficient wet electrostatic precipitator for removing nanoparticles, submicron and micron-sized particles", *Separation and Purification Technology*, **136**, 27–35.

GUO, B.Y., GUO, J. and YU, A.B., (2014), "Numerical modelling of electrostatic precipitation: effect of gas temperature", *J. Aerosol Sci*., **77**, 102-115.

GUO, B.Y., GUO, J. and YU, A.B., (2014), "Simulation of the electric field in wire-plate type electrostatic precipitators", *J. Electrostatics*, **72**, 301-310.

GUO, B.Y., SU, Y.B., YANG, D. and YU, A.B., (2015) "Modelling of gas flow and liquid spray in wet type electrostatic precipitators", *APCChE 2015, Chemeca 2015*, Oct, Melbourne.

GUO, B.Y., YANG, S.Y., XING, M., DONG, K.J., YU, A.B. and GUO, J., (2013), "Towards the development of an integrated ESP model", *I&ECR*, **52**, 11282−11293.

HITACHI, (2015), http://www.hitachi-plant-construction .com/product_solution/dustcollection/wet_type.html

ISHII, M. and ZUBER, N. (1979), "Drag coefficient and relative velocity in bubbly, droplet or particulate flows", *AIChE J*., **25**, 843-855.

LAWLESS, P.A., (1996), "Particle charging bounds, symmetry relations, and an analytic charging rate model for the continuum regime", *J. Aerosol Sci., 27*, 191-215.

SCHWINNING, G.M., (1998), "Wet ESPs, status and latest developments in the field of aerosol collection", *Proc. 7th Int. Conf. on Electrostatic Precipitation*, 522-533.

SENECAL, P. K., SCHMIDT, D. P., NOUAR, I. RUTLAND, C. J. and REITZ, R. D., (1999), "Modeling high speed viscous liquid sheet atomization", *Int. J. Multiphase Flow*, **25**, 1073–1097.

YAMAMOTO, I., YAMAMOTO, K., SHIMIZU, K. FUJIYAMA, Y., TSUNODA, K. and MIZUNO, A., (1998), "Wet type plasma reactor for incinerator", *Proc. IEEE IAS Annual Meet*., Oct., 1861–1864.